IET Microwaves, Antennas & Propagation

Research Article

IET Journals
The Institution of Engineering and Technology

Compact printed ultra-wideband diversity monopole antenna with slant inverted tree-shaped stub

ISSN 1751-8725
Received on 11th February 2015
Revised on 14th June 2015
Accepted on 16th June 2015
doi: 10.1049/iet-map.2015.0113
www.ietdl.org

Raj Kumar[1] ✉, *Neha Pazare*[2]

[1]*Department of Armament Electronics ARDE, Pashan, Pune-411 021, India*
[2]*Department of Applied physics, DIAT (DU), Girinagar, Pune-411 025, India*
✉ *E-mail: dr.rajkumarkumar@yahoo.com*

Abstract: A compact two-port diversity antenna is proposed and experimentally investigated. One of the ports is connected to a microstrip feed, whereas the other port to a coplanar waveguide feed. The radiating elements are semi-circular disc-shaped monopoles rotated around their centres. By shaping the common ground plane, ultra-wide impedance bandwidth is achieved. The measured bandwidths are 2–12 GHz at port 1 and 2.3–10.2 GHz at port 2. To obtain good isolation between the ports, a slant inverted tree-shaped structure is attached at the corner of the ground plane. The measured isolation is about 20 dB throughout the band. The antenna has omni-directional radiation patterns with a moderate peak gain of 2–7 dBi. To evaluate the diversity performance, the envelope correlation coefficient, diversity gain and capacity loss are calculated. A modified design with impedance bandwidth at port 2 extending beyond 11 GHz is also presented. The proposed diversity antenna is an attractive candidate to provide polarisation diversity and enhance channel capacity in a rich scattering environment.

1 Introduction

In recent years, a tremendous growth was witnessed in wireless communication technology. The wireless systems have a demand for high data-rate transmission with good signal quality that can be achieved with multiple-input–multiple-output antennas. Multiple antenna technology implements several antennas at the transmitter and receiver end of the wireless system to increase channel capacity. It also helps in reducing the signal fading in a multi-path environment and co-channel interference and thus improves the quality of the received signal. Diversity schemes can be realised in five different forms, namely: spatial, temporal, polarisation, frequency and pattern. When multiple antennas are placed closely to each other, for example, in a mobile platform, the problem of mutual coupling/isolation arises which is of prime importance. Hence, it is a challenge to design compact antennas with low mutual coupling.

Some of the recently proposed two-port antennas for diversity applications and with ultra-wide impedance bandwidth are shown in [1–12]. In these antennas, the basic arrangement consists of two radiating elements placed physically apart either side-by-side [1–6] or at right angles to each other [7–12]. While the former is used for pattern diversity, the latter is used for polarisation diversity. When they are placed side-by-side, the radiating elements are usually mirror images of each other which become more evident when they are not symmetric with respect to the feed line [3–6].

Among the two-port antennas where the elements are placed side-by-side, the isolation is usually provided by means of a metallic stub placed between the two. This stub acts as a reflector and reduces the coupling between the elements. In [1], the stub is inverted Y shaped and provides an isolation of about 15 dB for the antenna which has an impedance bandwidth from 3.2 to 10.6 GHz. A slightly larger antenna with a lower starting frequency (2.27 GHz) is described in [3]. Here, three stubs are placed between the Y-shaped radiating elements to provide a good isolation above 20 dB. A compact antenna covering the ultra-wideband (UWB) from 3.1 to 10.6 GHz is proposed in [4] and a T-shaped reflector is used to control the isolation to 15 dB. The radiating elements are square monopoles. Among the self-complementary monopoles [4–6], Roshna *et al.* [4] describes the use of a long metallic strip reflector to improve the isolation to more than 20 dB, [5] uses a tree-like structure, whereas in [6] a rectangular slot is cut in the ground plane. The isolation achieved in [5, 6] is more than 15 dB.

In the quadrature arrangement [7–12] the radiating elements can be simply rotated and placed side-by-side as in [7, 8] or one of them can be shifted upwards to achieve diagonal symmetry [9–12] which also brings the phase centres of the two ports closer to each other and nearer to the geometric centre of the antenna. The latter technique also ensures similarity in the two reflection coefficients. The isolating device used in [7] consists of two long metallic stubs protruding upwards from the ground plane and a short slit in the ground plane. The isolation achieved is 15 dB. In [8], only a slit in the ground is used to achieve the same amount of isolation for the antenna which is also more compact. When the radiating elements are placed in diagonal symmetry, the isolator invariably used is a cross-stub protruding from the ground plane to lie between the elements. Such an arrangement is not of advantage in case of [7, 8]. The isolating element in case of [9] is of stepped rectangular shape, in case of [10] has a fence shape, uses a cross-shape in [11] and a simple rectangular stub in [12]. The isolation achieved in all the cases is about 15 dB. A detailed comparison of the antennas [1–12] is presented in Table 1.

The antenna proposed comprises of two tilted semi-circular monopoles placed orthogonally and in a diagonally symmetric arrangement. One of the monopoles is microstrip fed, whereas the other is coplanar waveguide (CPW) fed. The impedance bandwidth obtained is from 2.3 to 10.2 GHz. The reflecting device used is a tree-shaped structure which gives about 20 dB isolation. In the following sections, the antenna physical details are provided followed by simulated and experimental results, parametric studies and performance analysis.

2 Antenna geometry

Fig. 1*a* shows the physical details of the proposed antenna, whereas Fig. 1*b* shows a photograph of the fabricated prototype. The antenna

© The Institution of Engineering and Technology 2015

Table 1 Comparison of the references; λ_0 – free space wavelength at the lowest operating frequency

Reference no.	Actual size, mm^2	Electrical size, λ_0^2	Bandwidth, GHz	Isolation, dB	Isolation technique used
[1]	40 × 68	1.28 × 0.72	3.2–10.6	15	Y-shaped stub
[2]	80 × 60	0.6 × 0.44	2.27–10.2	20	three rectangular stubs
[3]	22 × 36	0.23 × 0.37	3.1–10.6	15	T-shaped strip
[4]	25 × 30	0.26 × 0.31	3.1–10.6	20	long metallic strip
[5]	35 × 40	0.36 × 0.4	3.1–10.6	16	tree-shaped stub
[6]	21 × 38	0.21 × 0.39	3.1–10.6	15	rectangular slot in ground
[7]	26 × 40	0.26 × 0.4	3.1–10.6	15	long stub and slit in ground
[8]	32 × 32	0.33 × 0.33	3.1–10.6	15	slit in ground
[9]	48 × 48	0.37 × 0.37	2.3–11	15	stepped rectangular stub
[10]	43.5 × 43.5	0.45 × 0.45	3.1–10.6	15	fence-shaped stub
[11]	58 × 58	0.54 × 0.54	2.8–11	14	cross-shaped metallic strip
[12]	50 × 50	0.46 × 0.46	2.7–10.75	15	rectangular strip
proposed	40 × 40	0.31 × 0.31	2.3–10.8	20	tree-shaped stub

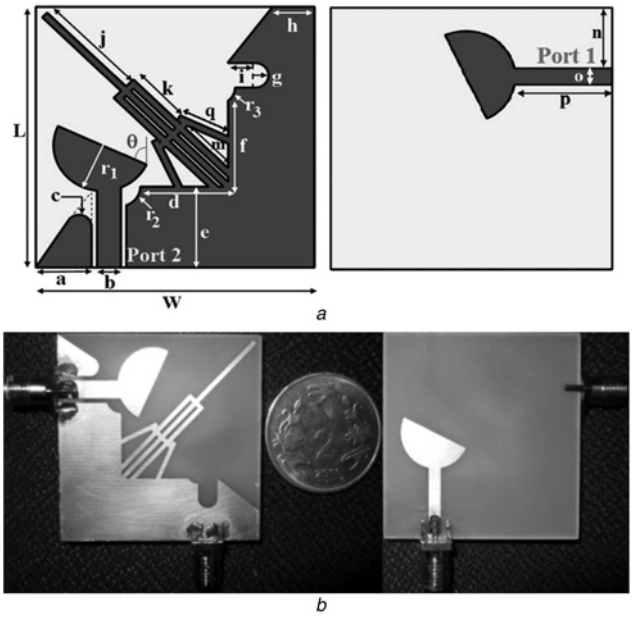

Fig. 1 *Proposed Antenna*

a Geometry of the top and bottom sides
b Fabricated prototype

is printed on both sides of a 40 mm × 40 mm flame retardant (FR-4) substrate having thickness of 1.6 mm, relative permittivity (ε_r) of 4.4 and loss tangent of 0.025. The radiating elements are semi-circular disc-shaped monopoles of radius 'r_1' millimetres. A circular geometry ensures multiple modes giving wider bandwidth and reduced mutual coupling [13], whereas the semi-circular structure is used to optimise space. The discs are rotated around their centres and make an angle of $\theta = 65°$ with the vertical. One of the discs is microstrip fed, whereas the other is CPW fed. This is done to combine the advantages of CPW feeding (such as less dispersion) and microstrip feeding (more design freedom). Moreover, it improves the isolation as shown in Fig. 2*d*. One half of the ground plane on the CPW side is triangular shaped with a blended upper corner. Similarly, half of the ground plane on the microstrip side is made trapezoidal. A small U-shaped slit is etched from the ground plane under the microstrip feed. An inverted tree-shaped metallic structure rotated by 45° and erected at the corner of the ground plane provides the isolation. The different sections of the tree have lengths given by '*j*', '*k*' and '*m*'. Each strip has a width of 1 mm and the strips of the middle and lower sections are separated by 0.5 mm. Furthermore, the strip '*q*' is rotated by 20° with respect to the central limb. A short-circuiting strip is placed at a height of '*m*' millimetres from the base of the tree. The different parameter values are listed in Table 2.

3 Simulated and measured *S*-parameters

The *S*-parameters of the antenna are measured using a vector network analyser (R & S ZVA-40) and compared with the simulated values in Figs. 2*a*–*c*. It is seen from the figures that the measured impedance bandwidth at port 1 is 2–12 GHz, whereas at port 2 is 2.3–10.2 GHz. The measured isolation between the ports is about 20 dB throughout the band as seen in Fig. 2*c*. A good agreement is noted between the simulated and measured results. In Fig. 2*d*, a comparison is made of coupling of the proposed antenna with the coupling that would have resulted if both the semi-circular discs have been CPW fed. It is seen that isolation is improved (particularly over 4–6 GHz) under hybrid feeding, that is, when the two feed lines are printed on the opposite sides of the substrate.

4 Evolution of diversity antenna with inverted tree-shaped stub

The various stages in the antenna design evolution and the performance optimisation achieved is illustrated by means of S_{21}, S_{11} and S_{22} curves in Fig. 3. The starting point of the antenna design is an antenna almost similar in structure to that shown in Fig. 1 but without the tree-shaped stub for isolation. Instead, for achieving isolation, a cross-shaped slot is cut in the ground plane at the corner. The *S*-parameter for this design is shown by line with star in Fig. 3. The impedance bandwidth is from 2.5 to 11.2 GHz for port 1 and 2.4 to 10.8 GHz for port 2. The isolation is better than 15 dB over the lower frequencies (2–6 GHz) and better than 20 dB over the upper frequencies (6–10 GHz). A dip in S_{11} and S_{22} is also observed near 1 GHz which can be said to be due to the common ground plane.

When a single slant stub is added and the cross-shaped slot stub at the corner and the semi-circular cut are removed, the isolation reaches 20 dB over most of the band (dashed line). As far as S_{11}/S_{22} are concerned, there is some deterioration over the middle frequencies. Moreover, the first resonance near 1 GHz shifts to the upper side. The isolation is further improved with the addition of the stubs forming the base of the tree (dotted line). However, during these changes, the return losses decrease near 4 and 6 GHz. To bring the S_{11} under –10 dB, additional slant stubs are attached at the base (dashed dotted line) and finally in the last stage a cross-stub is added shorting the lines (solid line). With this, good return loss characteristics along with isolation about 20 dB is obtained. This role of the tree-shaped stub is more evident from the comparison of current distribution plots of antennas with and without the tree-shaped stub shown in Fig. 3*d*. When the tree-shaped reflector is added to the structure, much of the current gets induced on it and less current is seen at the other port.

5 Parametric studies

In this section, results of some of the parametric studies carried out to assess the sensitivity of the antenna performance due to the various structural parameters are presented.

IET Microw. Antennas Propag., 2015, Vol. 9, Iss. 14, pp. 1595–1604
© The Institution of Engineering and Technology 2015

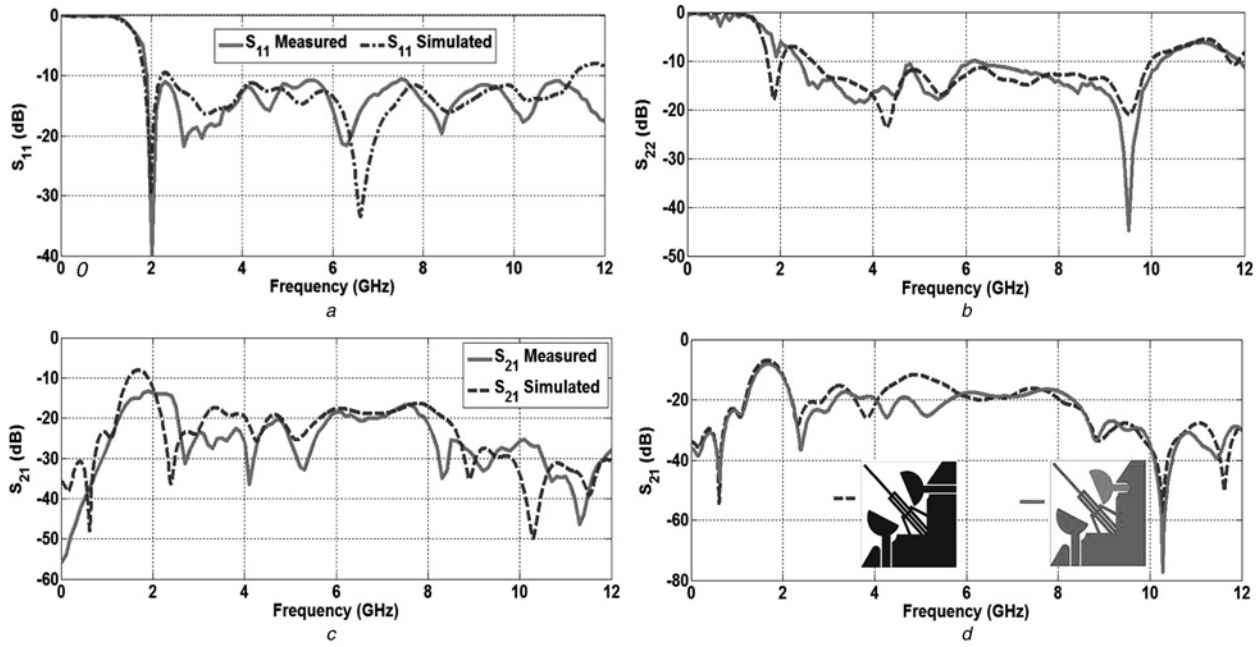

Fig. 2 *Isolation improvement*

a Measured/simulated S_{11}
b Measured/simulated S_{22}
c Measured/simulated coupling S_{21}
d Isolation comparison with similar feeding (both ports CPW feed) and hybrid feeding (one CPW feed and one microstrip feed)

5.1 Angle of inclination of semi-circular disc

At first, the angle which the semi-circular disc makes with the vertical, denoted by θ (theta) in Fig. 1 is varied and the effect on return loss and isolation is seen. As the angle is reduced (the discs are made more vertical), return loss increases near 6 GHz for port 1 and near 5 GHz for port 2. Hence, the value of the angle is optimised to 65° as shown in Fig. 4*a*. Very little effect on the isolation is seen due to the angle change although a slight decrease in isolation is noted near 8 GHz for a reduction in the angle.

5.2 Ground optimisation on the CPW side

The next parameter studied is the amount of blend done to the upper corner of the ground plane near the CPW side. This parameter is denoted by '*c*' in Fig. 1. The variation in S_{22} with blend is shown in Fig. 5*a*. As the blend is reduced, the return loss deteriorates over the lower frequencies (2–5 GHz) and improves near 7 and 10 GHz. On the other hand, an increase in the blend value will cause the return loss to deteriorate in the 6–8 GHz regions. Hence the value of the blend is optimised to 1.8 mm.

The height of the semi-circular patch on the CPW side is varied next and the variations in S_{22} are shown in Fig. 5*b*. The height, denoted by '*q*' in Fig. 5*b* is the distance between the base of the semi-circle and the ground plane edge. Its optimised value is 11.8 mm. This height controls the coupling between the radiating element and the ground plane. A decrease in the height causes a decrease in the return loss over 5–8 GHz, whereas an increase deteriorates it over 8–9 GHz. The return loss at lower frequencies is unaffected.

Table 2 Optimised dimension of antenna (millimetres)

Label	Size	Label	Size	Label	Size	Label	Size
a	8	*b*	3.4	*c*	1.8	*d*	12.6
e	12.4	*f*	13.2	*g*	1.9	*h*	6
i	3.6	*j*	17	*k*	9.5	*m*	10.5
n	9.25	*o*	2.5	*p*	13.9	*L*	40
W	40	*q*	6.5				

5.3 Ground optimisation on the microstrip side

The height of the right side ground edge on the microstrip side is denoted by '*h*' in Fig. 1. It is varied to see the effect on S_{11} and the results are shown in Fig. 6*a*. As the height is increased, that is, the ground plane becomes more rectangular than trapezoidal, there is a decrease in the return loss near 5 GHz. Moreover, some mismatch is seen near 2.5 and 7.5 GHz. As the height is reduced, the mismatch appears at 4 GHz. Hence, the height is optimised to 6 mm. The parameter varied next is the height of the semi-circular patch above the ground plane on the microstrip side denoted by '*p*' in Fig. 1. Its optimised value is 13.9 mm. As stated before, this height controls the coupling between the radiating element and the ground plane. A decrease in the height from its optimised value causes a decrease in the return loss over the lower frequencies, near 5 GHz and from 9 to 11 GHz. On the other hand, an increase in the height increases the return loss over these frequencies. Finally, the depth of the U-shaped slot etched in the ground plane under the microstrip feed is varied and the results shown in Figs. 6*c* and *d*. As the slot depth is decreased, the return loss deteriorates near 8 GHz and improves over the upper frequencies. There is also a deterioration in S_{11} and isolation near 5 GHz. On the other hand, a larger depth improves S_{11} and isolation near 5 GHz. Finally, the value of the depth is optimised to 5.5 mm.

6 Radiation patterns, efficiency and group delay

6.1 Radiation patterns

The measured radiation patterns of the proposed antenna in the *E*-plane and *H*-plane at four different frequencies in the operating band are compared and shown in Fig. 7. The radiation patterns in the *E*-plane are dumb bell shaped and the *H*-plane are omni-directional in shape. The *H*-plane patterns at port 1 and port 2 are also found to be slightly complementary (for example, at

© The Institution of Engineering and Technology 2015

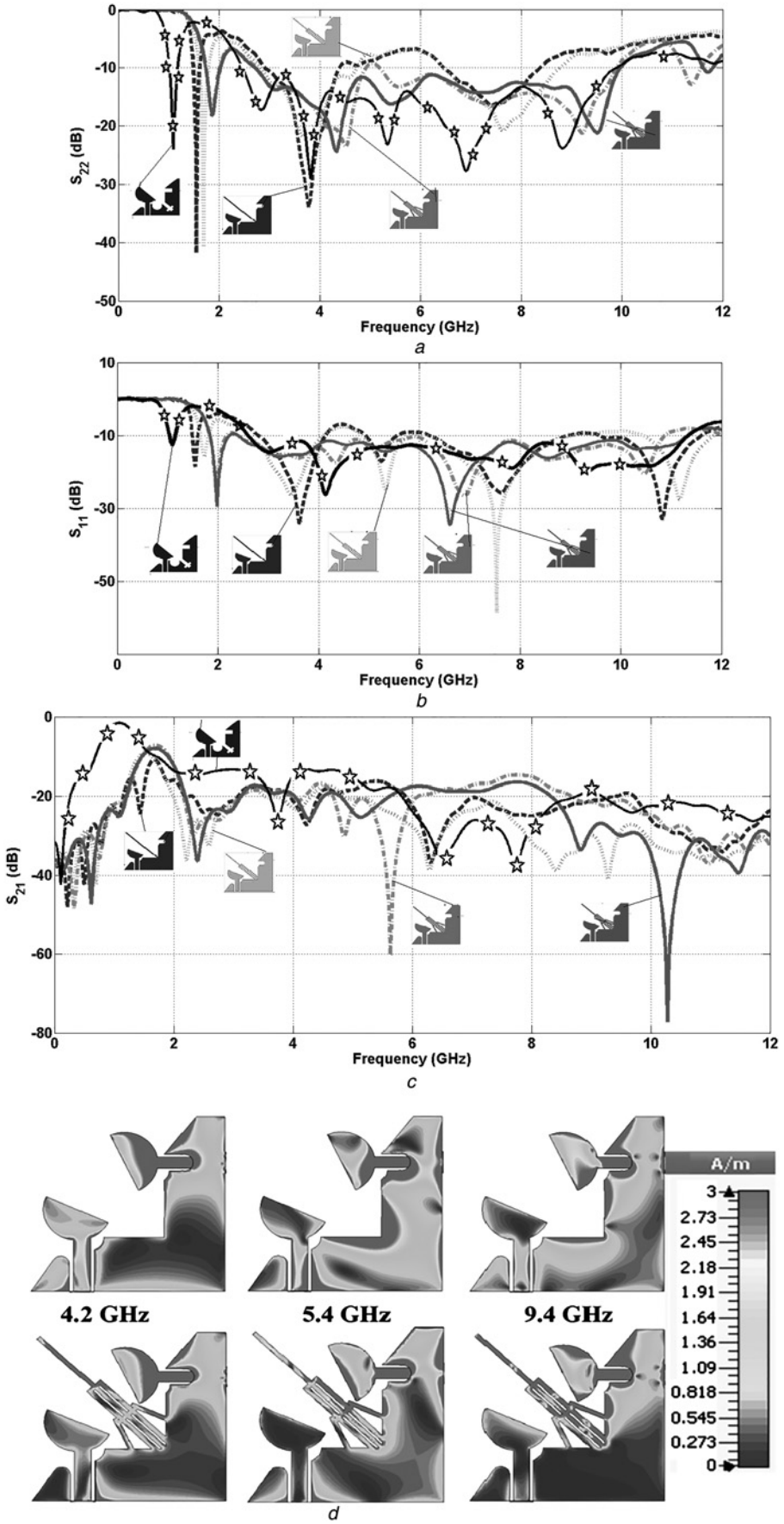

Fig. 3

a Simulated S_{11}
b Simulated S_{22}
c Simulated S_{21} due to various stages of modifying the inverted tree-shaped stub
d Current distribution with/without the tree

© The Institution of Engineering and Technology 2015

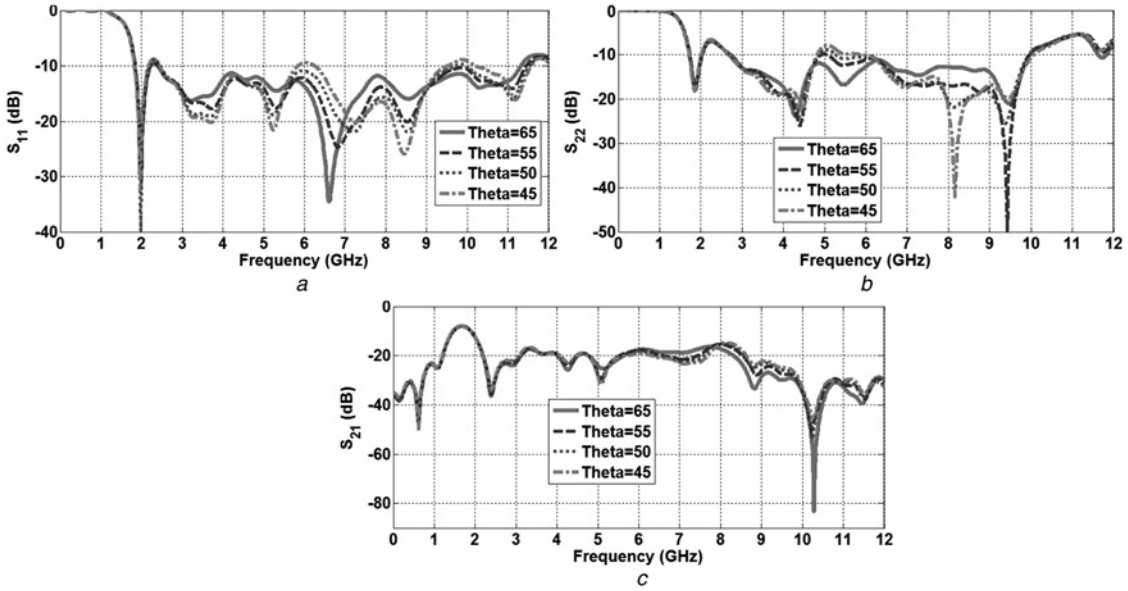

Fig. 4 *Simulated results of*

a S_{11}
b S_{22}
c S_{21} for different values of semi-circular patch inclination 'theta'

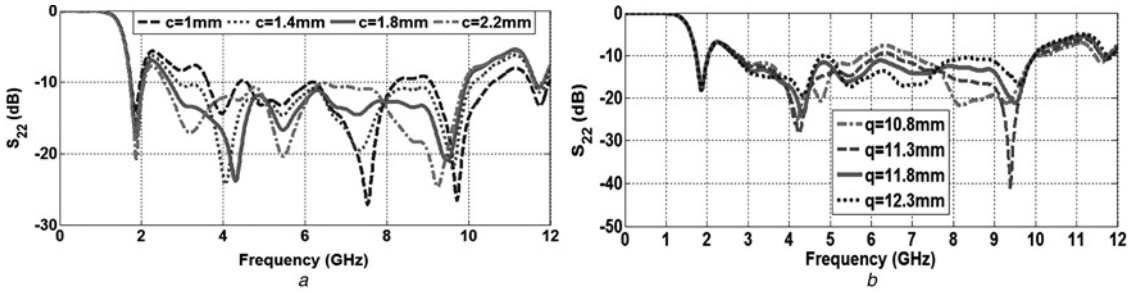

Fig. 5 *Variations in* S_{22} *with respect to change in*

a Ground corner blending (CPW side)
b Height of the semi-circular patch above the ground (CPW side)

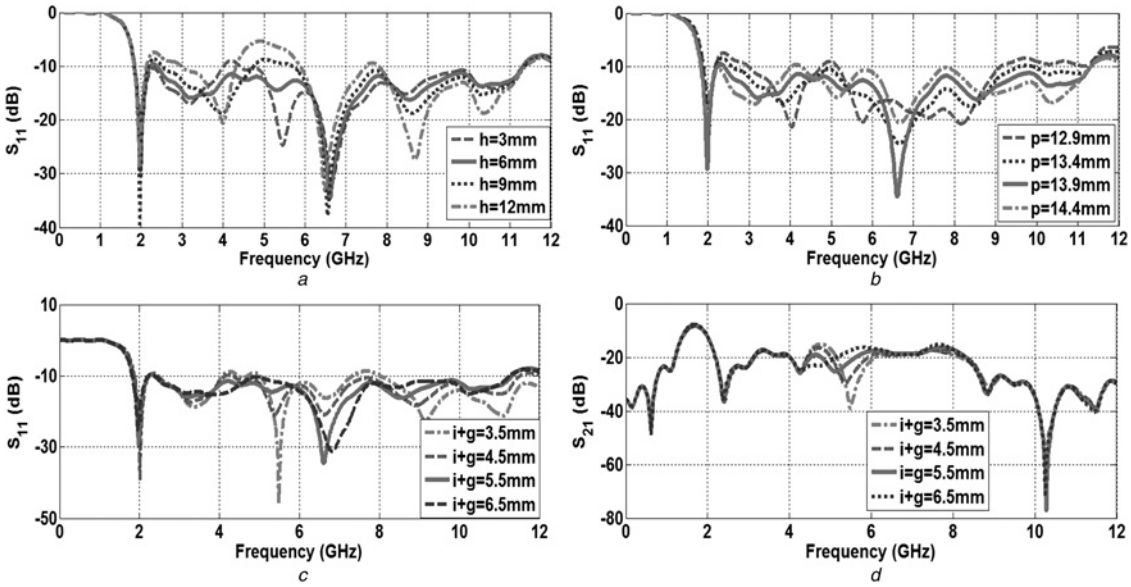

Fig. 6 *Variations in*

a S_{11} with ground edge height on microstrip side
b S_{11} with height of semi-circular patch above the ground on microstrip side
c S_{11}
d S_{21} with depth of U-shaped slot under the microstrip feed

© The Institution of Engineering and Technology 2015

6 GHz). This is because for port 1, the *H*-plane happens to be the *YZ*-plane, whereas for the port 2 the *H*-plane is the *XZ*-plane. A little asymmetry seen in the radiation patterns can also be attributed to the asymmetry in the ground plane (difference between the left and right ground plane halves). A plot of the measured and simulated peak gains at both the ports is shown in Figs. 8*a* and *b*. The peak gain varies between 2 and 7 dBi over the operating band. An increase in the gain seen at upper frequencies is due to an increase in the antenna effective area.

The simulated radiation efficiencies are in Fig. 8*c*. Both the efficiencies remain above 75% over the operating band. The reduction in the efficiency at higher frequencies is due to an increase in the frequency-dependent copper and substrate losses. To assess the time-domain performance, the group delay is measured which checks the phase linearity and pulse distortion. It is obtained as the first differential coefficient of the phase. Fig. 8*d* shows the measured group delay with the antennas placed face-to-face and side-by-side at a separation of 30 mm. It can be seen from the figure that the group delay variations is between 0.5 to 1ns over the entire bandwidth which indicates the good time domain performance of the antenna.

7 Diversity performance

To evaluate the diversity performance of the proposed antenna, diversity parameters are computed in both uniform and non-uniform environments. One of the important parameters is the envelope correlation coefficient (ECC) which is a measure of the correlation between the signals received at the two ports. It indicates the decoupling between the ports and can be calculated from the far-field radiation patterns using (1) [14]. Its value should be <0.5 [13] (see equation (1) at bottom of the next page)

$$P_{\theta}(\theta,\ \phi) = A_{\theta} \exp\left[\frac{-\left\{\theta - \left(\frac{\pi}{2} - m_{v}\right)\right\}^{2}}{2\sigma_{v}^{2}}\right], \quad (0 \le \theta \le \pi) \quad (2a)$$

$$P_{\phi}(\theta,\ \phi) = A_{\phi} \exp\left[\frac{-\left\{\theta - \left(\frac{\pi}{2} - m_{H}\right)\right\}^{2}}{2\sigma_{H}^{2}}\right], \quad (0 \le \theta \le \pi) \quad (2b)$$

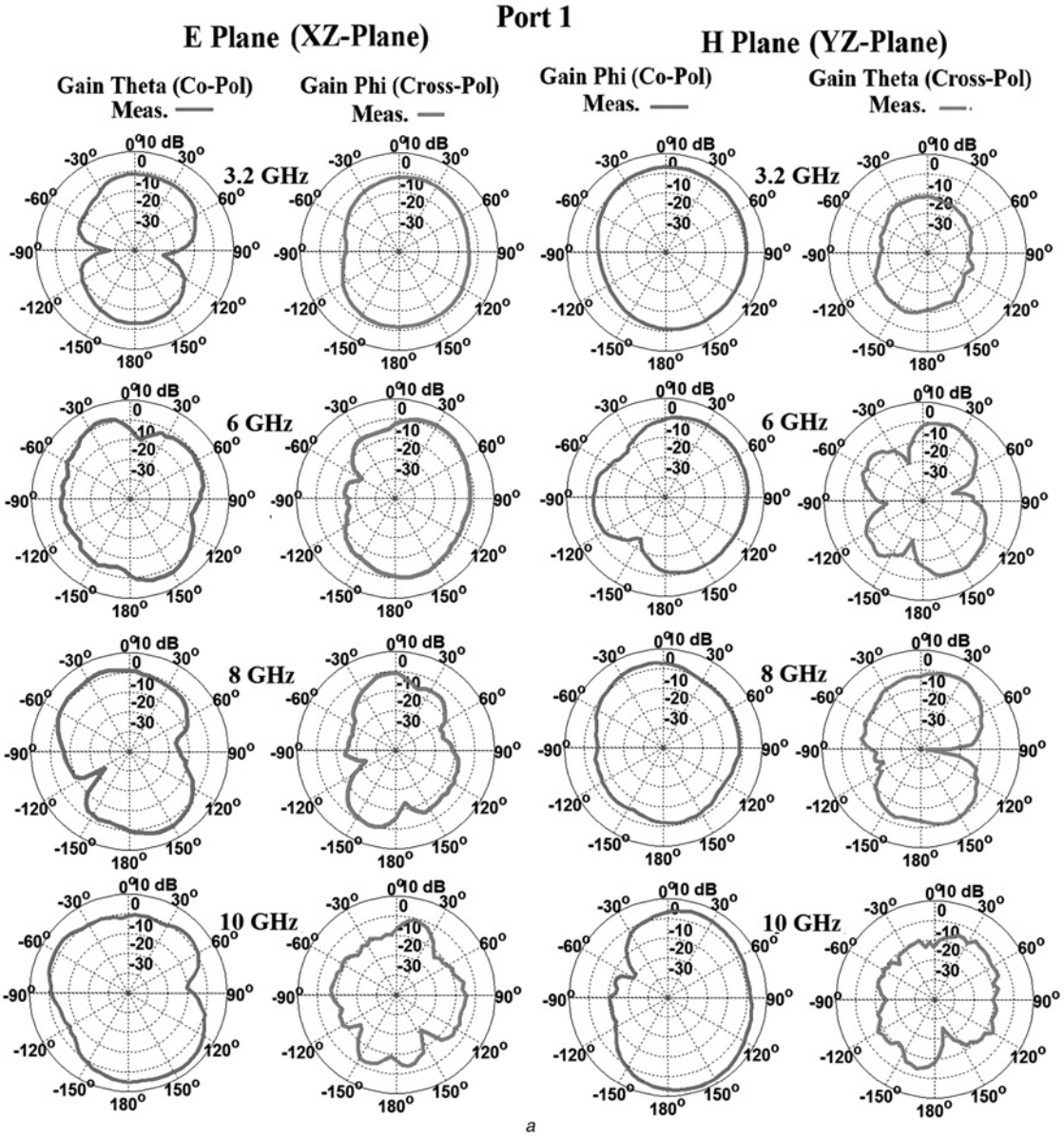

Fig. 7 *Measured and simulated radiation patterns*

a Port 1
b Port 2

IET Microw. Antennas Propag., 2015, Vol. 9, Iss. 14, pp. 1595–1604
© The Institution of Engineering and Technology 2015

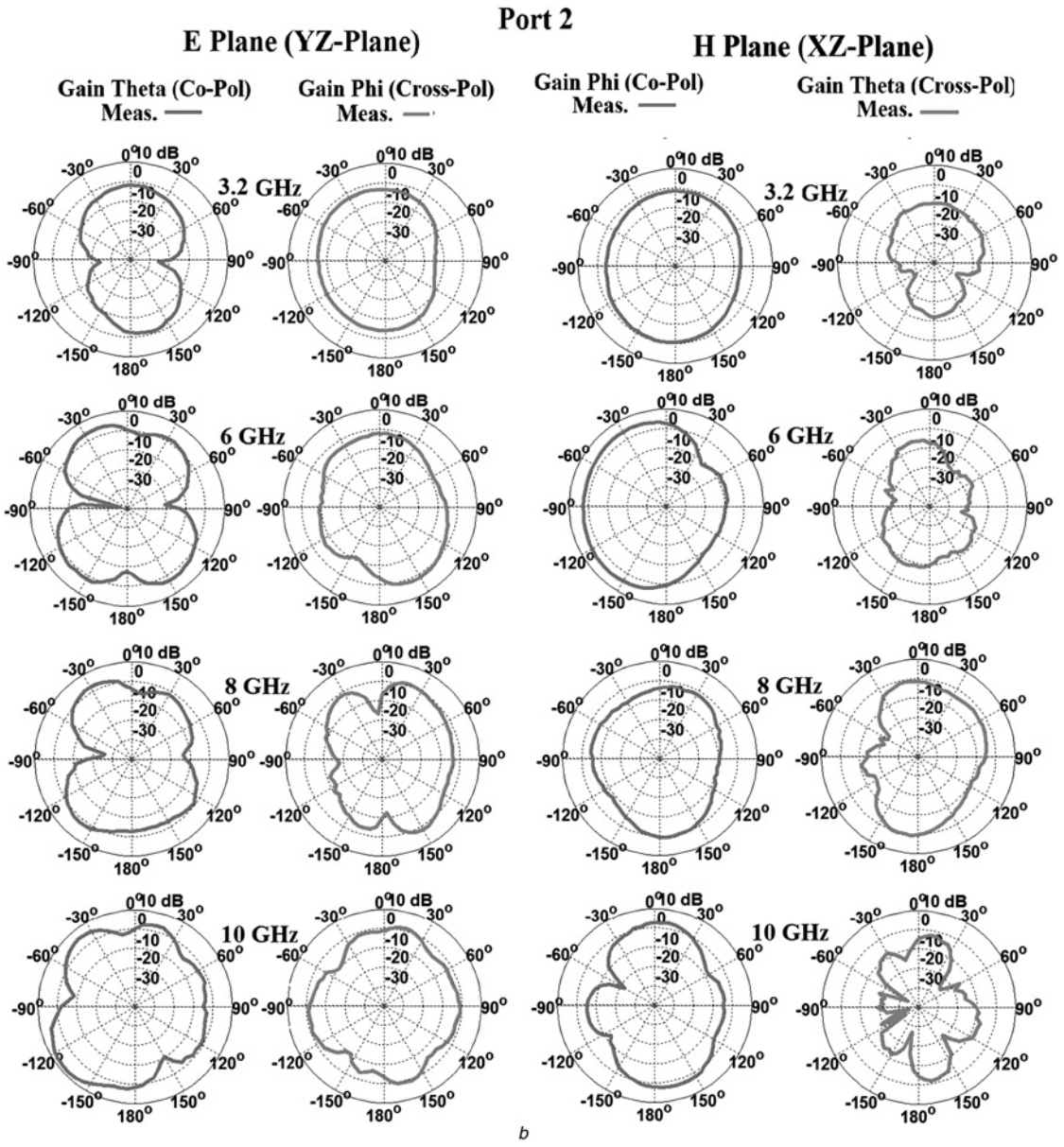

Fig. 7 *Continued*

$$\int_0^{2\pi}\int_0^{\pi} P_\theta(\theta,\ \varphi)\sin\ \theta\,\mathrm{d}\theta\,\mathrm{d}\varphi = \int_0^{2\pi}\int_0^{\pi} P_\varphi(\theta,\ \varphi)\sin\ \theta\,\mathrm{d}\theta\,\mathrm{d}\varphi = 1 \quad (3)$$

In (1), cross polarisation ratio (XPR) is the environment-dependent cross-polarisation ratio, G_θ, G_ϕ are the power gain patterns and P_θ, P_ϕ are the components of angular density functions of the incident power given by (2a) and (2b). A_θ and A_ϕ are constants to be determined by (3) [15]. In the present study, we have chosen P_θ, P_ϕ to be Gaussian/uniform distributed in the elevation/azimuth directions so that the mean (m_v, m_h) and standard deviations (σ_v, σ_H) of the elevation of the incident wave's θ and ϕ component will be as given in Table 3. Furthermore, in regard to XPR, four different environments, namely: isotropic, indoor, outdoor and wireless world initiative new radio (WINNER) are studied. The WINNER interface was developed as a project under the framework programme (FP6) of the European commission and is a part of the wireless world initiative. WINNER II is the latest in the initiative and models the mobile communication environment for both short range and wide area. The XPR values as given in [14, 16] are listed in Table 3. The simulated ECC curves for the various models are shown in Fig. 9*a*.

In case of a uniform environment, the ECC can also be calculated from *S*-parameters using (4) [14]. Another parameter related to the ECC is the diversity gain (DG). It is the increase in signal-to-noise ratio due to diversity combining for a given level of cumulative probability or reliability [17]. It can be obtained from the ECC

$$\rho_{ij} = \left| \frac{\oiint \mathrm{XPR}\cdot E_{\theta i}(\Omega)\cdot E^*_{\theta j}(\Omega)\cdot P_\theta(\Omega) + E_{\varphi i}(\Omega)\cdot E^*_{\varphi j}(\Omega)\cdot P_\varphi(\Omega)\,\mathrm{d}\Omega}{\sqrt{\oiint \mathrm{XPR}\cdot G_{\theta i}(\Omega)\cdot P_\theta(\Omega) + G_{\phi i}(\Omega)\cdot P_\phi(\Omega)\,\mathrm{d}\Omega \cdot \oiint \mathrm{XPR}\cdot G_{\theta j}(\Omega)\cdot P_\theta(\Omega) + G_{\phi j}(\Omega)\cdot P_\phi(\Omega)\,\mathrm{d}\Omega}} \right|^2 \quad (1)$$

© The Institution of Engineering and Technology 2015

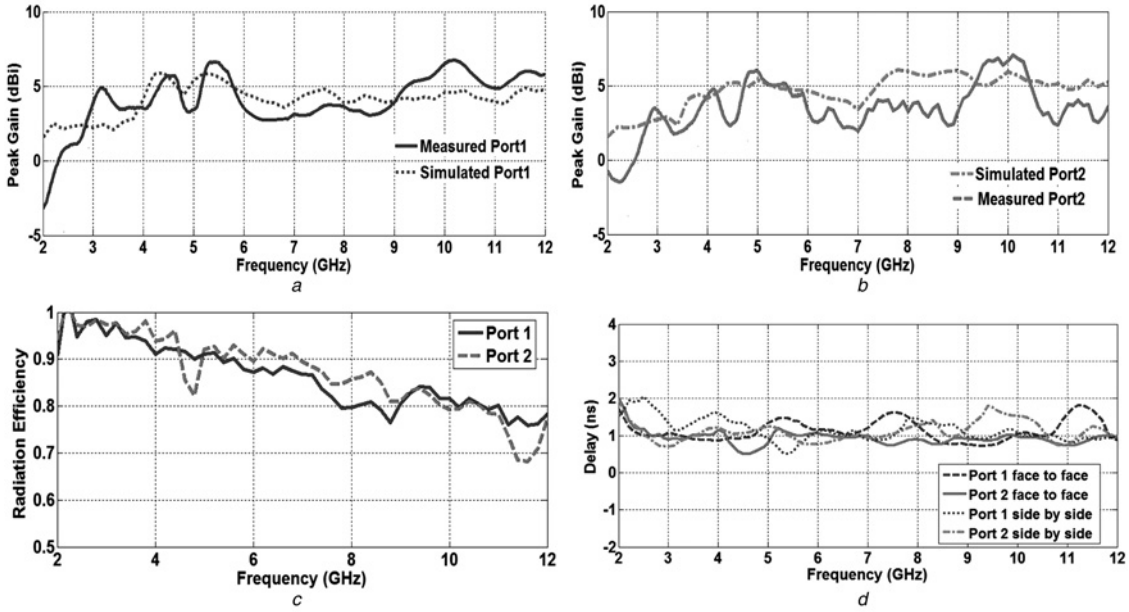

Fig. 8 *Plot of the measured and simulated peak gains at both the ports*

a Simulated/measured peak gain at port 1
b Simulated/measured peak gain at port 2
c Simulated radiation efficiencies
d Measured group delay

Table 3 Propagation parameters used to evaluate the performance of the antenna system

Parameter	Uniform/isotropic	Indoor	Outdoor	WINNER II
m_V, m_H, deg	10	10	10	10
σ_V, σ_H, deg	15	15	15	15
XPR, dB	0	1	5	9

using (5). The ECC and DG values calculated from the simulated and measured *S*-parameters are shown in Fig. 9*b*. The ECC (from the radiation patterns as well as from the *S*-parameters) has a low value (<0.06) and DG is close to 10 which promise good diversity performance

$$\rho = \frac{\left|S_{11}^{*}S_{21} + S_{12}^{*}S_{22}\right|^2}{\left|\left(1 - \left|S_{11}\right|^2 - \left|S_{21}\right|^2\right)\left(1 - \left|S_{22}\right|^2 - \left|S_{12}\right|^2\right)\right|} \tag{4}$$

$$G = 10\sqrt{1 - |\rho|} \tag{5}$$

The third parameter considered is the mean effective gain (MEG) which is the ratio of the average received power at any port of the antenna over an arbitrary route to the total mean power incident at the antenna terminals. It is also calculated from far-field radiation patterns using 6 [15] and the simulated values for different environments are shown in Fig. 9*c*. For the WINNER interface which is a more realistic model, the MEG has a smaller value which also corresponds to a higher value of the ECC. Ideally, the MEGs at the two ports should be equal but a difference of 3 dB between the MEGs is considered acceptable in a practical environment [14]. From Fig. 10*c*, it can be seen that the difference between the MEGs at the two ports is small up to 10 GHz where after it increases. This is possibly because the two antennas are not exactly identical and have a difference in their reflection coefficients as well (Figs. 2*b* and *c*). The worst-case difference between the MEGs is seen to be 2 dB (at 11 GHz)

$$\text{MEG} = \int_0^{2\pi}\int_0^{\pi}\left[\frac{\text{XPR}}{1+\text{XPR}}G_\theta(\theta,\ \phi)P_\theta(\theta,\ \phi) + \frac{1}{1+\text{XPR}}G_\phi(\theta,\ \phi)P_\phi(\theta,\ \phi)\right]\sin\theta\,\mathrm{d}\theta\,\mathrm{d}\phi \tag{6}$$

The last parameter considered is the capacity loss. It represents the loss in transmission capacity when compared with an arrangement where the antenna elements are used to form an array and calculated from *S*-parameters by using (4) [18]. The simulated and measured capacity losses shown in Fig. 10*d* are below 0.6 bps/Hz. This confirms that a good return loss and low mutual coupling between two antenna elements leads to a low ECC and low capacity loss

$$C_{\text{loss}} = -\log_2|A| \tag{7}$$

where $A = \begin{bmatrix}\rho 11 & \rho 12\\ \rho 21 & \rho 22\end{bmatrix}\rho_{ii} = 1 - (|S_{ii}|^2 + |S_{ij}|^2)\ \rho_{ij} = -(S_{ii}^{*}S_{ij} + S_{ji}^{*}S_{ji})$, for $i = j = 1$ or 2.

8. Modified design for improved return loss

A difference in the reflection coefficient characteristics at the two ports is seen from Fig. 2 which is because of the difference in the feed structures. The impedance bandwidth at port 1 extends beyond 11 GHz, whereas for Port 2 it is only up to 10 GHz. To make the impedance bandwidth at both the ports cover the UWB range from 3.1 to 10.6 GHz, the antenna geometry is modified as shown in Fig. 10*a*. Basically, the arc-shaped cut in the ground plane to the right side of the CPW feed is replaced by a

IET Microw. Antennas Propag., 2015, Vol. 9, Iss. 14, pp. 1595–1604
© The Institution of Engineering and Technology 2015

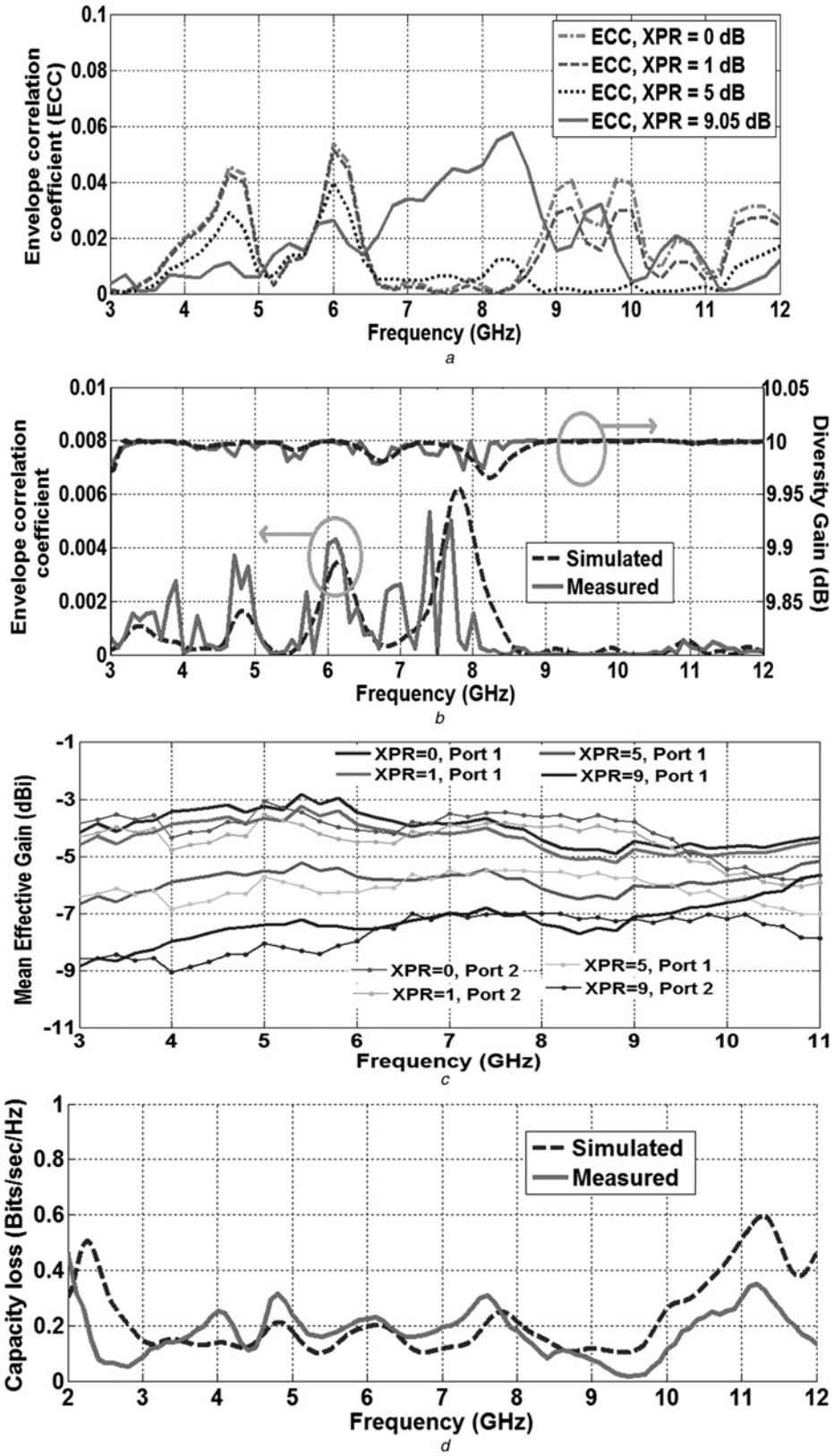

Fig. 9 *Simulated ECC curves for the various models*

a Simulated ECC for different propagation environments from far-field radiation patterns
b ECC and DG from simulated and measured *S*-parameters
c Simulated MEG
d Simulated and measured capacity loss

semi-circular cut of radius 1.3 mm. The centre of the semi-circle is displaced by 0.3 mm from the upper ground edge and by 2.2 mm from the left ground edge. The simulated *S*-parameters for this design are shown in Figs. 10*b*–*d*. It is seen that as a result of the modification, the impedance bandwidth at port 2 is extended to 11.5 GHz without any major effect on the isolation.

© The Institution of Engineering and Technology 2015

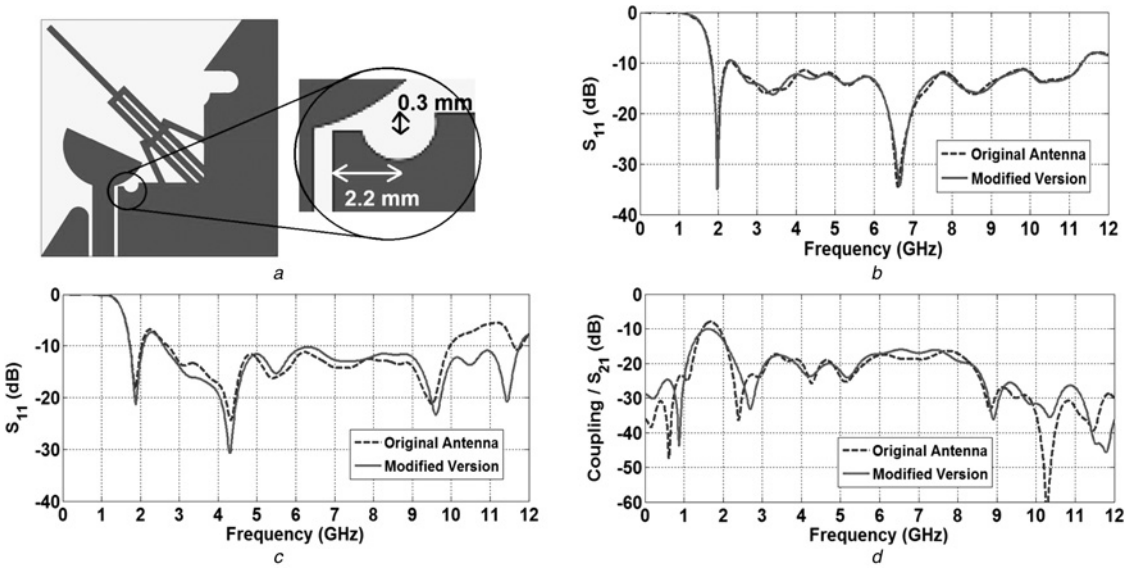

Fig. 10 *Modified design*

a Geometry
b S_{11}
c S_{22}
d Coupling S_{21}

9 Conclusions

A compact and miniaturised diversity antenna is proposed. It consists of two monopoles shaped in the form of semi-circular discs and rotated around their centres. The measured impedance bandwidths of 2–12 GHz for port 1 and 2.3–10.2 GHz for port 2 has been achieved by modifying the common ground plane at several places by means of cuts and edge blends. The isolation is improved throughout the band to about 20 dB by placing an inverted tree-shaped stub at the ground plane corner. The antenna has complementary radiation patterns at the two ports. The diversity features such as correlation coefficient, MEG and capacity loss are calculated and found to have acceptable values. A modified design with impedance bandwidth at port 2 extending beyond 11 GHz is also presented. The antenna will be useful for UWB applications requiring diversity features as in high data-rate communications with increased reliability.

10 References

1 Najam, A., Duroc, Y., Tedjni, S.: 'UWB-MIMO antenna with novel stub structure', *Prog. Electromagn. Res. C*, 2011, **19**, pp. 245–257
2 Hong, S., Chung, K., Lee, J., Jung, S., Lee, S., Choi, J.: 'Design of a diversity antenna with stubs for UWB applications', *Microw. Opt. Lett.*, 2008, **50**, (5), pp. 1352–1356
3 Liu, L., Cheung, S.W., Yuk, T.I.: 'Compact MIMO antenna for portable UWB applications with band-notched characteristic', *IEEE Trans. Antennas Propag.*, 2015, **63**, (5), pp. 1917–1924
4 Roshna, T.K., Deepak, U., Sajitha, V.R., Vasudevan, K., Mohanan, P.: 'A compact UWB MIMO antenna with reflector to enhance isolation', *IEEE Trans. Antennas Propag.*, 2015, **63**, (4), pp. 1873–1877
5 Zhang, S., Ying, Z., Xiong, J., He, S.: 'Ultrawideband MIMO/diversity antennas with a tree-like structure to enhance wideband isolation', *IEEE Antennas Wirel. Propag. Lett.*, 2009, **8**, pp. 1279–1282
6 Liu, L., Cheung, S., Yuk, T.: 'Compact multiple-input–multiple-output antenna using quasi-self-complementary antenna structures for ultrawideband applications', *IET Microw. Antennas Propag.*, 2014, **8**, (13), pp. 1021–1029
7 Liu, Li, Cheung, S.W., Yuk, T.I.: 'Compact MIMO antenna for portable devices in UWB applications', *IEEE Trans. Antennas Propag.*, 2013, **61**, (8), pp. 4257–4264
8 Ren, J., Hu, W., Yin, Y., Fan, R.: 'Compact printed MIMO antenna for UWB applications', *IEEE Trans. Antennas Propag.*, 2014, **13**, pp. 1517–1520
9 Huang, H., Liu, Y., Zhang, S., Gong, S.: 'Uniplanar ultrawideband polarization diversity antenna with dual band-notched characteristics', *IEEE Antennas Wirel. Propag. Lett.*, 2014, **13**, pp. 1745–1748
10 Qin, H., Liu, Y.: 'Compact UWB MIMO antenna with ACS-fed structure', *Prog. Electromagn. Res. C*, 2014, **50**, pp. 29–37
11 Chacko, B.P., Augustin, G., Denidni, T.A.: 'Uniplanar slot antenna for ultrawideband polarization-diversity applications', *IEEE Antennas Wirel. Propag. Lett.*, 2013, **12**, pp. 88–91
12 Chacko, B., Augustin, G., Denidni, T.: 'Uniplanar polarisation diversity antenna for ultrawideband systems', *IET Microw. Antennas Propag.*, 2013, **7**, (10), pp. 851–857
13 Kharche, S., Reddy, G.S., Mukherjee, B., Gupta, R., Mukherjee, J.: 'MIMO antenna for Bluetooth, Wi-Fi, Wi-MAX and UWB applications', *Prog. Electromagn. Res. C*, 2014, **52**, pp. 53–62
14 Karaboikis, M., Papamichael, V., Tsachtsiris, G., Soras, C., Makios, V.: 'Integrating compact printed antennas onto small diversity/MIMO terminals', *IEEE Trans. Antennas Propag.*, 2008, **56**, (7), pp. 2067–2078
15 Singh, H., Meruva, B., Pandey, G., Bharti, P., Meshram, M.: 'Low mutual coupling between MIMO antennas by using two folded shorting strips', *Prog. Electromagn. Res. B*, 2013, **53**, pp. 205–221
16 Kyösti, P., Laselva, D., Hentilä, L., Jämsä, T.: 'Validating IST-WINNER indoor MIMO radio channel model'. IST Mobile and Wireless Summit, Mykonos, Greece, June 2006
17 Dietrich, C., Dietze, K., Nealy, J., Stutzman, W.: 'Spatial, polarization, and pattern diversity for wireless handheld terminals', *IEEE Trans. Antennas Propag.*, 2001, **49**, (9), pp. 1271–1281
18 See, C., Abd-Alhameed, R.A., Abidin, Z.Z., McEwan, N.J., Excell, P.S.: 'Wideband printed MIMO/diversity monopole antenna for WiFi/WiMAX applications', *IEEE Antennas Wirel. Propag. Lett.*, 2012, **60**, (4), pp. 2028–2035

© The Institution of Engineering and Technology 2015

Copyright of IET Microwaves, Antennas & Propagation is the property of Institution of Engineering & Technology and its content may not be copied or emailed to multiple sites or posted to a listserv without the copyright holder's express written permission. However, users may print, download, or email articles for individual use.